Journal of
Materials Chemistry C

Materials for optical and electronic devices

ROYAL SOCIETY
OF CHEMISTRY
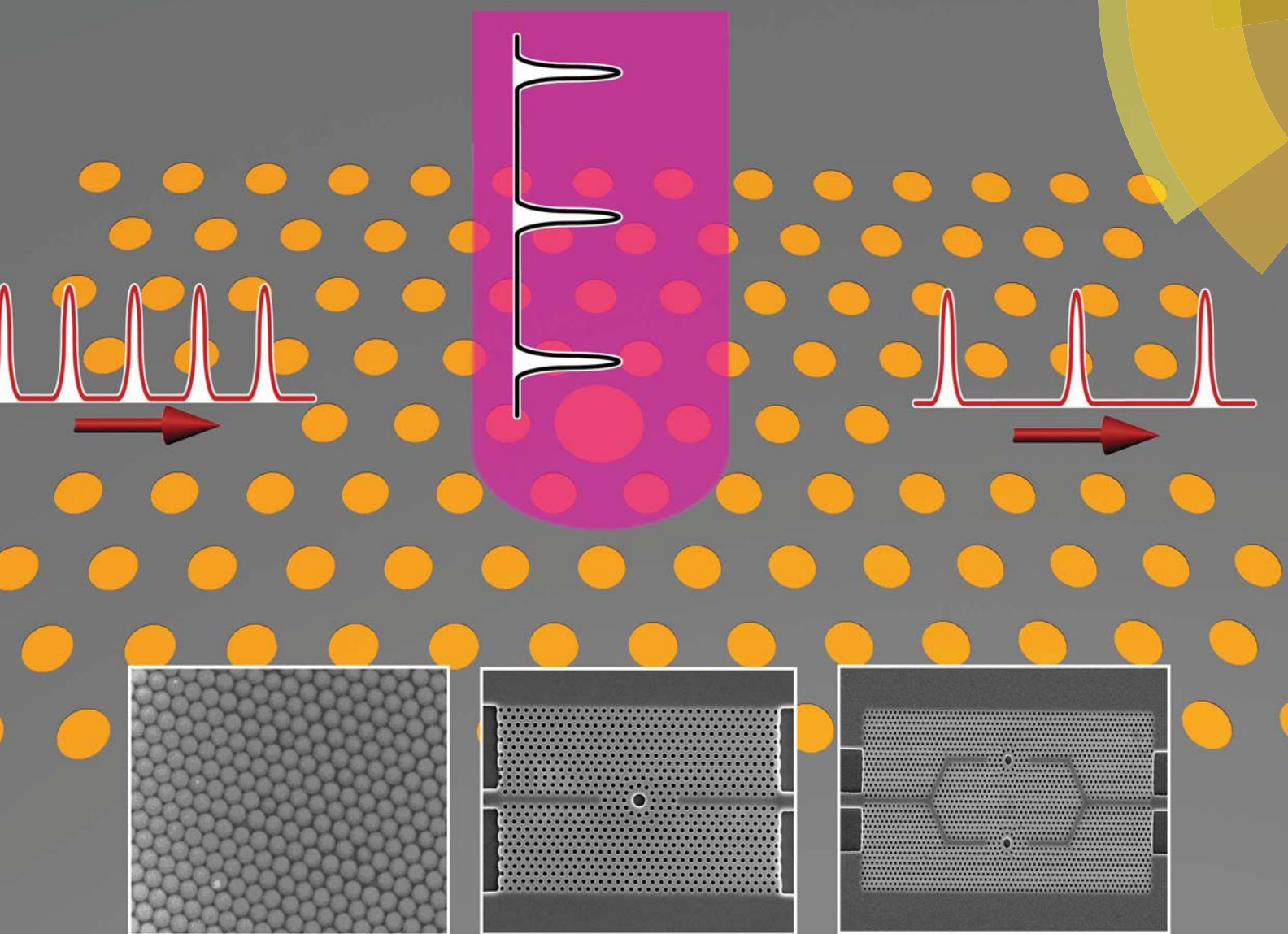
FEATURE ARTICLE
Zhi-Yuan Li and Zi-Ming Meng
Polystyrene Kerr nonlinear photonic crystals for building ultrafast optical
switching and logic devices

FEATURE ARTICLE

Polystyrene Kerr nonlinear photonic crystals for building ultrafast optical switching and logic devices

Zhi-Yuan Li*[a] and Zi-Ming Meng[b]

In recent years all-optical switching and logic devices have received extensive attention due to their potential applications in next generation ultrahigh-speed information processing and optical computing. Kerr nonlinear photonic crystals (NPC) offer a promising route to realize all-optical switching with ultrafast response time and low pump power based on simple and robust physical mechanisms. In this feature article, we present our extensive investigation on Kerr NPCs made from polystyrene, an organic polymer material with large Kerr nonlinearity and extremely fast response time down to several femtoseconds, and their application to build ultrafast, low power, and high contrast optical switching and logic devices. Several relevant issues are discussed and analyzed, including the principal working mechanism of all-optical switching and logic devices in Kerr NPCs, preparation of polystyrene NPCs by means of microfabrication and self-assembly techniques, characterization of optical switching performance by means of femtosecond pump-probe technique, and synthesis of silicon–polystyrene hybrid NPCs by means of nano-imprint technology as a promising route to construct switching, modulating, and logic devices compatible with popular silicon photonics.

1. Introduction

Ultrafast all-optical processing and computing are highly desired in today's ever increasing large data consuming era, which exhibits a promising alternative to break the limitation of electronic circuits. Currently, two of the most daunting

[a] *Laboratory of Optical Physics, Institute of Physics, Chinese Academy of Sciences, P. O. Box 603, Beijing 100190, P. R. China. E-mail: lizy@aphy.iphy.ac.cn; Fax: +86 10-8264 9356*

[b] *School of Physics and Optoelectronic Engineering, Guangdong University of Technology, Guangzhou 510006, P. R. China*

This journal is © The Royal Society of Chemistry 2014

J. Mater. Chem. C, 2014, **2**, 783–800 | **783**

problems preventing significant increases in the microelectronic processor speed are thermal and signal delay issues associated with electronic interconnection. Optical interconnects, on the other hand, possess an almost unimaginably large data carrying capacity, and may offer interesting new solutions for circumventing these problems. A photon is a good carrier for information and energy because it has much a faster transfer speed, better parallel degree, and more capabilities as a frequency carrier than an electron. All-optical switching is an essential component in all-optical processing, computing and networking. Compared with traditional electro-optical switching, all-optical switching has the obvious advantage of ultra-fast time response, which meets the need of high speed information processing. Much research has concentrated on this aspect for a long time. Several materials, ranging from dielectrics to semiconductors and organics, have been investigated to characterize their linear and nonlinear properties for all-optical switching. Friberg et al.[1] reported the first demonstration of a nonlinear dual-core fiber coupler switch capable of substantially complete all-optical switching at subpicosecond rates. Almeida et al.[2,3] realized an all-optical switching on a silicon chip by the structure of ring resonator. Sasaki et al.[4,5] proposed an all-optical switching in a composite thin film of silver and polymer matrix containing photochromic dye.

For a practical all-optical switching four points should be considered. They are high switching efficiency, i.e. high intensity contrast between two states of "ON" and "OFF," low switching power, fast switching time, and utility for integrated optical circuits. A tremendous amount of work has been paid to the realization of all-optical switching trying to satisfy all the four strict conditions at the same time. The photonic crystal (PC), firstly proposed by Yablonovitch[6] and John[7] in 1987, can control the propagation of electromagnetic waves in the same way as periodic potential in a semiconductor crystal affects the electron motion by defining allowed and forbidden electronic energy bands. By introducing nonlinear optical materials into PC structures, the optical properties can be tuned by an external drive, such as a strong pump laser. This tunable property is important for all-optical switching or modulators. Nowadays, much research of all-optical switching has turned to nonlinear photonic crystal (NPC) structures, which involve Kerr nonlinear materials within the structure. In theory, Fan et al.[8] proposed an analytic theory to study the switching dynamics in PC microcavities. Soljacic et al.[9] investigated properties of hybrid systems of PC microcavities incorporating a highly nonlinear ultraslow light medium, and found that such systems can enable ultrafast nonlinear all-optical switching at ultralow (even single photon) energy levels. In experiment, Tanabe et al.[10] reported an all-optical switching in the telecommunication band with extremely low switching energy (a few 100 fJ), high switching contrast (about 10 dB), and high speed (about 50 ps) on the silicon chip by using PC nanocavities. Hu et al.[11] reported ultrafast and low-power PC all-optical switching based on strong optical nonlinearity enhancement due to excited-state inter-electron transfer. The switching operation power is reduced by four orders of magnitude, and the ultrafast response time is in the order of one picosecond.

PC structures based on semiconductor materials are considered to be one of the most excellent candidates in fabricating nanoscale integrated all-optical circuits. However, the relatively weak and slow nonlinear optical properties of pure semiconductor materials have hindered the further progress in reducing the consumption power or pulse energy and the response time. Quite recently sub-femtojoule all-optical switching using a semiconductor PC nanocavity has been demonstrated.[12] Nevertheless, the total switching time is still in the tens of picoseconds due to the carrier-induced nonlinearity. Compared with the traditional semiconductor materials, such as silicon, InP, or GaAs, conjugated organic molecules and polymers[13,14] possess a relatively large third-order nonlinear susceptibility and femtosecond response time, which are of great importance to the realization of all-optical switching. Note that the third-order optical nonlinear susceptibility is in the order of 10^{-12} cm^2 W^{-1} for usual conjugated organic molecules and 10^{-14} cm^2 W^{-1} for traditional semiconductor materials. Moreover, by introducing dye molecules[11,15,16] or gold nanoparticles[17] into the polymer thin films, the third-order nonlinear susceptibility will become even larger.

Although the conjugated polymer materials such as polystyrene hold excellent third-order optical nonlinearity, the microfabrication technology for building polymeric PC structures are not so sophisticated compared to that for semiconductor materials. In this paper we discuss our recent progress in building high-quality polystyrene Kerr NPCs by using microfabrication technology and self-assembly method and their application in realizing ultrafast all-optical switching. Our works can be approximately divided into two categories. On one hand we have made great efforts to continually increase the optical switching speed to its limit for the two-dimensional (2D) and three-dimensional (3D) polystyrene NPCs. On the other hand we have successfully fabricated high-quality semiconductor–polymer compound PC slab and air-bridged polymer PC slab, which show great potential in achieving integrated all-optical switching and logic devices on the nanoscale. The arrangement of this article is as follows. In Section 2 we present the fundamental physical principles of all-optical switching in NPCs with several different operation routines. In Section 3 we discuss several materials science schemes to realize NPC structures for all-optical switching application. The detailed experimental preparations, arrangements and measurements in 2D and 3D NPC all-optical switching are shown in Sections 4 and 5, respectively. In Section 6 we present how to fabricate high-quality semiconductor–polymer compound 2D NPC slabs by using nano-imprint lithography technique. The fabrication of high-quality air-bridged polymeric 2D NPC slab is discussed in Section 7. In Section 8 we show how optical logic devices can be realized based on our polymeric 2D NPC slab. Finally we conclude this feature article in Section 9.

784 | J. Mater. Chem. C, 2014, 2, 783–800

This journal is © The Royal Society of Chemistry 2014

2. Principles and schemes for all-optical switching in nonlinear photonic crystals

Generally speaking, all-optical switching in NPCs can be classified into two kinds. In the first kind, the switching exploits the nonlinearity of the material by controlling the intensity of the input signal, and this utilizes a sort of self-switching effect where the input pulse will trigger optical switching by itself. In the second kind, the nonlinearity is exploited by launching a control beam to trigger optical switching for the input signal which can maintain a relatively low level of intensity. NPCs provide new mechanisms to realize all-optical switching based on different nonlinear effects. In the following, several mechanisms which are usually used in PC structures are analyzed, which include photonic band gap (PBG) edge shift, defect mode shift, optical bistability effect, and two-photon absorption effect.

According to the basic electromagnetic theory of PCs, the band gap is strongly dependent on the refractive index of each composite material. So for a NPC with a composite material exhibiting Kerr nonlinearity, the refractive index will change dynamically under the incident high-intensity pump beam according to a simple linear law as $n = n_0 + n_2 I$.[18] Here n is the refractive index at a given pump light intensity of I, n_0 is the refractive index in the absence of pump light, and n_2 is the Kerr nonlinearity coefficient of the composite material. This Kerr effect will lead to the shift of the photon band gap,[19–21] as illustrated in Fig. 1(a). When the signal light is just located at the band gap edge, its transmission energy will change dynamically with respect to the pump beam as the signal light either sees the pass band with high transmissivity (called the "ON" state) under no pump light or the band gap with low transmissivity (called the "OFF" state) under pump light. The contrast in the transmission signal intensity will realize the "ON" and "OFF" state of an optical switching. More interestingly, as the optical switching is driven by the external pump light, the major properties of the switching, which are the response speed and switching contrast, can be well controlled by the intensity and pulse duration of the pump light. Suppose that the nonlinear material has a very fast (say, almost instantaneous) optical response to the driven light, the response time of the switching should be in the order of the duration time of the pump light pulse. This means that it is possible to utilize a state-of-the-art ultrashort pulse laser technique, in particular the femtosecond laser technique, to realize a super-fast switching speed (down to a few femtoseconds) that is several orders of magnitude larger than the traditional optoelectronic switching (tens of picoseconds).

There is another unique property of PCs – existence of localized defect modes that are easy to engineer and control.[22–24] When a defect is intentionally introduced into the periodic arrays in an appropriate way, a high transmission state will appear in the band gap with a sharp and narrow resonance peak, and this corresponds to a defect mode. The defect state will also shift with the change of refractive index. Similar to the
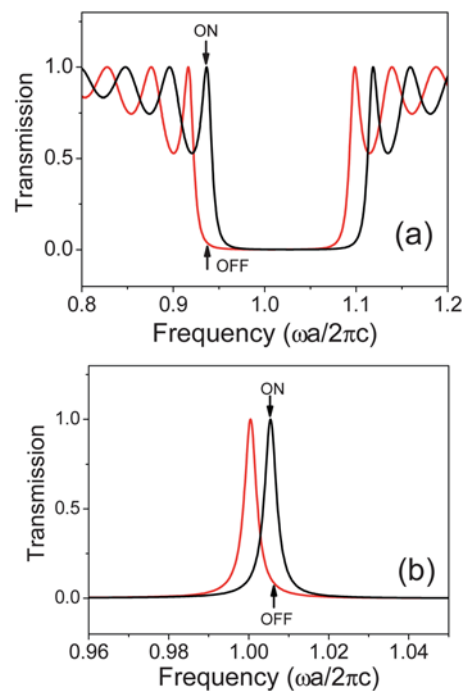
Fig. 1 Principle of optical switching in NPCs. Schematic picture of optical switching utilizing (a) the band gap edge shift and (b) defect mode shift under the high-intensity pump light upon a Kerr NPC. Black and red curves correspond to the transmission spectrum before and after external pump light. As the Kerr nonlinear material has an increased refractive index, the spectrum red shifts to lower frequency when the external pump light is turned on. The arrows denote the probe light frequency position, which will be on the high transmission state (ON state) and low transmission state (OFF state) before and after pump light, and this can be harnessed to build an optical switching device.

situation of band gap edge shift, the shift of the defect state can also be exploited as a controllable optical switching under external pump light. Such a picture is depicted in Fig. 1(b). By suitable design, the defect mode shift can be made to be much more sensitive than the band gap edge shift upon a tiny change of refractive index. This may be very useful to reduce the pump power of all-optical switching.

Optical bistability is an important effect for many nonlinear optical devices. When this effect is combined with PCs, it has shown a promising prospect for optical switching. A system with optical bistability has two stable resonant transmissions states, dependent on the input and the history, and this feature can be utilized to serve as an optical switch, which basically belongs to the category of self-switching. Two factors should be satisfied in the nonlinear system: nonlinear interaction between the nonlinear material and input optical field, and the feedback process. In a PC with Kerr nonlinearity, a resonant cavity can serve as the basis for optical bistability. Nonlinear coupling between the input light, which might transport through a single-mode PC waveguide, and the cavity will lead to optical bistability exerting the feedback effect. All-optical switching in NPCs based on optical bistability has been studied theoretically.[8,22,25–30] A great advantage for a PC cavity is that a high quality (Q) factor nanocavity can be designed at

This journal is © The Royal Society of Chemistry 2014

J. Mater. Chem. C, 2014, **2**, 783–800 | **785**

will and realized experimentally, and this can greatly lower the input light power level that is sufficient to initiate considerable optical bistability. Nonetheless, due to the difficulty to create a NPC with strong enough Kerr nonlinear coefficient and accessible infrared signals with high enough power level at the nanoscale, the concept of optical bistability switching in PCs has yet to be demonstrated experimentally even with the help of signal enhancement in a high-Q resonant cavity.

The two-photon absorption effect[31–33] can also be used to realize all-optical switching in PCs.[34] The usual materials which possess a large two-photon absorption cross section are mostly semiconductors, such as silicon, GaAs, and some organic polymers. This makes it possible to realize two-photon absorption optical switching in semiconductor PCs with good band gap and defect mode performance. One way to achieve ultrafast optical switching in silicon is by exploiting its ultrafast nonlinear optical properties. The idea is to increase the density of free carriers in silicon and enhance its refractive index by using an intense ultrashort laser pulse at the electronic band-edge of silicon. Optically excited electrons and holes induce ultrafast alteration of the refractive index in silicon, causing a shift in the optical Bragg diffraction of the PC from its original position[35] or shift in the resonant frequency of a PC microcavity. Nowadays, many researchers have demonstrated the properties of all-optical switching with two-photon absorption in silicon.[34,36,37] Nonetheless, the free-carrier absorption effect has a limit in the response time, which is in the order of sub-nanosecond. This makes it difficult to pursue much faster optical switching speed that is well below sub-picosecond level by this two-photon absorption scheme.

The optical bistability scheme and two-photon absorption scheme rely merely on the input light signal to generate a nonlinear optical effect that is sufficiently strong to induce a jump between "ON" and "OFF" states of PC resonant modes. This requires either strong Kerr optical nonlinearity or large two-photon absorption cross sections. This has brought about a serious problem in the material part. As light signal transporting in a PC integrated circuit is usually weak, currently it is difficult to trigger observable self-switching effect in the nanoscale system made from usual semiconductor materials.

Taking this difficulty into full account, in the past years our work has been focused on design, realization, and characterization of ultrafast all-optical switching in NPCs under external pump light of femtosecond laser pulse with very high peak power level but with only modest average power. We have successfully demonstrated efficient optical switching based on band gap edge shift or defect state shift in 2D and 3D NPCs with a response time scaled down to a few femtoseconds. In addition, we have made extensive efforts to build integrated NPC optical switching and logic devices on the platform of silicon–polystyrene 2D NPC slab or polystyrene 2D NPC slab.

3. Nonlinear optical materials for all-optical switching

The above discussions on the physical principles for different schemes of optical switching in NPCs have clearly indicated the importance of appropriate nonlinear optical materials for realizing high performance all-optical switching. Three main types of nonlinear materials have been extensively used in tunable PCs: dielectrics, semiconductors, and polymer materials. Among the different dielectric materials, ferroelectric inorganic crystals or silica fiber have been demonstrated to hold large nonlinearities. However, some aspects hinder their application in ultrafast all-optical switching.[38–40] One feature is the constraint of working with only single crystalline materials. Another is the relatively slow optical switching time, which is in the millisecond range. A third is the difficulty in creating microscale/nanoscale all-optical switching devices that will be placed in the background of an integrated optical circuit. So our work is concentrated on the semiconductor and polymer materials for building ultrafast all-optical switching, especially the semiconductor–polymer compound structures exhibiting the advantages of possessing ease of integration and excellent Kerr nonlinearity simultaneously.

Semiconductor materials have played a great role in the microelectronic technologies, and they are now also a very good platform for creating PC integrated devices and chips because of their relatively large refractive index in the telecommunication wavelength. Nowadays, all-optical switching and modulators have been demonstrated with III–V compound semiconductors.[41,42] For silicon, a more popular and important semiconductor material, it is harder to achieve the same performances of all-optical switching due to its relatively weak optical nonlinearity and bad optoelectronic properties. Despite the difficulties, more and more efforts have been made on the silicon or silicon-on-insulator (SOI) structures[2,35,43,44] in order to realize all-optical switching on silicon PC structures.

The basic nonlinear effect on semiconductor materials is the two-photon absorption. As a result, the speed of these all-optical switches is limited by the effective carrier relaxation time, whose value is sub-nanosecond for silicon micro-ring cavities[2] and about 100 ps for line defect PC nanocavities.[10] The relaxation time can be shortened by ion implanted semiconductors, which allows a faster switching recovery time for PC optical switching. Recently, Tanabe et al.[45] reported an all-optical switching with the response time of 70 ps using ion-implanted silicon PC nanocavities. Further downscale of the optical switching response time will encounter enormous difficulties.

Due to the development of synthetic, physical and theoretical chemistry, organic polymer materials have attracted much attention. Organic polymer materials are of major interest because of their relatively low cost, easy fabrication and integration into devices, higher laser damage threshold, fast nonlinear optical response time, and off-resonance nonlinear optical susceptibilities comparable to or exceeding those of ferroelectric inorganic crystals.[13] In the field of PC all-optical switching, the widespread nonlinear polymer materials include liquid crystals, polystyrene, polymethyl methacrylate (PMMA), and polyphenylene vinylene (PPV). An earlier tunable PC in experiment[46] primarily focused on electro-optic and

786 | J. Mater. Chem. C, 2014, 2, 783–800

This journal is © The Royal Society of Chemistry 2014

thermo-optic band edge tuning *via* infiltrated liquid crystals since Busch and John proposed the concept of a tunable PC by means of infiltrating a liquid crystal into the void regions of an inverse opal PC structure.[47] However, the molecular reorientation processes responsible for changes in the refractive index of liquid crystals typically occur in a time scale ranging from milliseconds to seconds, and this strictly prohibits rapid band edge tuning. In regard to obtaining an ultrafast response speed, polystyrene,[11,48,49] PMMA, and PPV have received much consideration due to the benefits of femtosecond response time and relatively large third-order nonlinear susceptibility in these polymer materials. In addition to the aforementioned three types of nonlinear materials, there are still some new artificial materials that are exploited to realize all-optical switching. These include metal materials with surface plasmon effect[50] and quantum dot[51] or quantum well materials with optical tunability through nonlinearity.

In the past decade, we have carried out a series of experiments on all-optical switching in PC structures made from the nonlinear material of polystyrene. We have made extensive efforts to continually push-up the optical switching response time to its limit. In 2003, our first experiment[52] was demonstrated in an organic 3D polystyrene opal PC structure, whose response time is several picoseconds. However, the transmission contrast, which is an important evaluation index for optical switching, is as low as 8% with the peak intensity of pump laser as 14.4 GW cm^{-2}. With improvement of the quality of PC sample, the band gap edge becomes steeper, which reduced the pump intensity and increased the transmission contrast. In 2005, we realized all-optical switching with the response time of 10 ps in 2D polystyrene PC structures, which was based on the principle of band gap edge shift[48] and defect mode shift.[53] The transmission contrast was as high as 65%. We also realized all-optical switching[49] in a 3D polystyrene opal structure in the same year, whose response time was as short as 120 fs, and the contrast was about 45% under the pump intensity of 27.5 GW cm^{-2}. An all-optical switching with 20 fs response time was then demonstrated in 2D polystyrene PC in 2006.[54] In 2007, we fulfilled an all-optical switching of 10 fs in a 3D polystyrene opal NPC system. In the following sections we will discuss briefly these investigations.

4. All-Optical switching in two-dimensional nonlinear photonic crystals

Since the basic physical phenomenon of a PC is based on Bragg scattering in periodic lattice structures, the repeating regions of high and low dielectric constants have to be of the same length scale as half the wavelength of electromagnetic waves. So for the visible or infrared wave, the length scale of scattering units is in the order of 100 nm, which brings a major challenge for the fabrication of 2D and 3D PC structures. Nowadays, with the rising development of micro-fabrication technology and other micro/nano manipulation and characterization technologies, it is a relatively easy task to fabricate 2D PCs and various devices.

In our 2D polystyrene PC experiment, we use polystyrene powder with normal molecular weight of 8 million (Fluka Chemie Company, Switzerland). Firstly, the polystyrene powder is dissolved in toluene with a weight ratio of about 1 : 100. The spin coating method,[55] which is a preferred method for application of thin, uniform films to flat substrates, is then used to fabricate a thin film slab of polystyrene on a quartz substrate, which is pre-cleaned carefully. The thickness of the thin film is about 300 nm, which is measured by a surface profiler (Model Dektek 8, DI Company, USA). Changing the concentration of polystyrene toluene solution, or changing the rotating speed during the spin coating process, the thickness of the thin film will be changed. We can select optimized experimental conditions as desired. Finally, a focused ion beam etching (FIB) system (Model DB235, FEI Company, USA) is employed to prepare the periodical patterns of 2D PC. Before etching the periodical patterns, a thin gold layer with thickness of about 15 nm is sputtered onto the surface of the polystyrene film, which is used to make up for the weak electrical conductivity of polystyrene. After the etching process, the thin gold layer is wiped off by the potassium iodide (KI) solution where the weight ratio of iodine (I$_2$), potassium iodide and distilled water is 1 : 1 : 4. In addition, as the required periodical patterns are much larger than the area that we can finish in one single FIB treatment, (the required patterned area is about 3 μm × 100 μm, while the area which we can etch by FIB is about 10 μm × 10 μm) so the multiple screen joint technology is used during the process of etching by FIB. By this method, good quality PC samples are fabricated.

With the 2D polystyrene NPC at hand, we continue to characterize its optical properties. For this purpose, we have built a high-efficiency experimental setup for characterizing the performances of all-optical switching in 2D NPCs. In order to introduce the incident light into our PC thin film structures, three major coupling techniques which are widely used in 2D PCs can be used, implementing the prism coupling, the fiber coupling, and the grating coupling. Prism coupling[48,56] is a traditional but effective method to realize the coupling between incident light and optical thin film. It is based on the principle of evanescent field coupling. The incident light is totally reflected at the prism base, and under certain conditions,[57] light energy can be transferred into the film by optical tunneling. This method is very simple, easy to operate, and it is suitable for PC structures with a relatively large area.

In our experiment, the prism coupling method is used to realize the input and output of polystyrene thin films. The pump–probe technique is used to measure the ultrafast optical switching signals. A typical experiment setup is depicted in Fig. 2(a). Two laser pulses (either from the same pulse laser or from two different pulse lasers) are usually used in this experiment. Their parameters, such as the wavelength, pulse duration, pulse repetition, or the energy of the pump pulse, can be tuned according to the design. The optical delay line, which is actually a precision positioning stage, is introduced to the pump light path to adjust the optical length difference between

This journal is © The Royal Society of Chemistry 2014

J. Mater. Chem. C, 2014, **2**, 783–800 | **787**
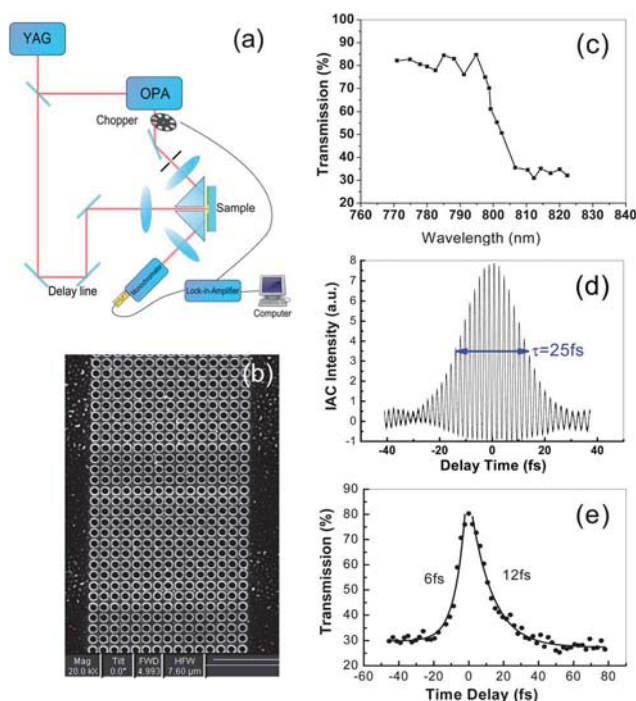
Fig. 2 Experimental characterization of 20 fs optical switching in a 2D NPC. (a) Schematic configuration of the experimental setup for two-dimensional photonic crystal optical switching. (b) SEM image of the photonic crystal and (c) measured linear transmission spectrum, which indicates the band gap edge located at about 800 nm. (d) Interferometric autocorrelation signals of the pump pulse laser beam, showing a pulse duration of about 25 fs. (e) Measured transmittance change depending on the time delay between pump and probe beams. The solid lines represent the exponential fits of the experimental points.

the pump and probe laser pulses. The output signals from the prism-film coupling system are detected by a monochromator, amplified by a photomultiplier tube, and finally received by the lock-in amplifier which is controlled by a computer. There are three lenses in the optical path, which are used to focus the pump light, the input and output probe light that couple with the prism. In addition, except for a beam splitter, many total reflection mirrors are used to reduce the loss of laser energy. By this experimental arrangement, we can measure the linear or nonlinear transmission spectra and the time response with different pump energies for 2D NPCs. Most of our all-optical switching experiments in 2D NPCs are performed with this system by only changing the parameters of the incident pump or probe lasers according to our needs.

Polystyrene, as an organic conjugated polymer, possesses a relatively large third-order nonlinear susceptibility and very fast (down to a few femtoseconds, almost instantaneous) response time. From the above analysis, the optical switching response time of the NPC is mainly limited by the time resolution of experimental measurements that is largely determined by the duration of pump pulse. So if the pump and probe pulses are significantly shortened down to the femtosecond scale, the femtosecond response time of all-optical switching may be achieved. Based on this consideration, a homemade Ti:sapphire

laser (TFS-1, Institute of Physics, Chinese Academy of Sciences) with the pulse duration and pulse repetition rates of 25 fs and 80 MHz was used as the incident probe and pump pulse. Because the central wavelength of Ti:sapphire laser is located at around 800 nm, the optimized lattice constant and the hole radius were found via numerical simulation to be 350 and 115 nm, respectively, for which the band gap of the PC is near 800 nm.[54] The scanning electron microscopy (SEM) image and measured linear transmission spectrum of this PC are shown in Fig. 2(b) and (c), respectively, which agrees well with the numerical simulation. The measured interferometric autocorrelation signals of the pump pulse laser beam are illustrated in Fig. 2(d), showing a pulse duration of about 25 fs.

The optical switching demonstrated in 2D polystyrene NPC adopted the scheme of band gap shift.[54] The experimental setup was similar to that shown in Fig. 2(a) except that the OPA system was replaced by a total reflection mirror and a beam splitter with the intensity ratio of 1 : 9 was used to separate the incident laser pulse into the pump and probe pulses. Thus, the pump and probe lights used to measure the optical switching properties have the same wavelength. The pump light had a peak intensity of about 13 GW cm^{-2}. In the experiment, the probe light was selected to have a wavelength of 806 nm, which is located at the short-wavelength band edge of the PC. The synchronization of the two femtosecond pulses with the duration of 25 fs was also needed before recording the experimental data. For this aim, a finer stage was used in the arm of the optical delay line. The measured time delay curve of optical switching signals is shown in Fig. 2(d). The all-optical switching of the polystyrene PC has reached an ultrafast response time of 20 fs, which is measured from the full width at half maximum (FWHM) of the time delay curve. The transmittance contrast is from 33% to 78% when the system changes from the "OFF" state to the "ON" state.

The above optical switching is based on the principle of the band gap edge shift. The performance of the devices will be largely influenced by the quality of PC samples. If the periodicity is very good, the band gap edge will be very steep, which in turn will make a larger switching contrast under the same or even lower pump power. Generally speaking, a defect mode will provide a steeper edge than the band gap edge in the PC system due to its fine resonance nature. For this reason, in our works we also paid much attention to all-optical switching based on the defect mode shift in NPCs. In 2005 we showed the all-optical switching with the response time of 10 ps in a 2D polystyrene PC with a defect.[53] In this experiment, the 1064 nm laser (with a pulse duration and pulse repetition rate of 20 ps and 10 Hz, respectively) from YAG laser (Model PL2143B, Ekspla Ltd., Lithuania) was used as the pump light, while a laser (pulse duration 10 ps and repetition rate 10 Hz) from an OPA (Model OPA-740, CAS) with the wavelength range from 450 nm to 650 nm and pumped by the same YAG laser was used as the probe laser. We first designed a structure whose defect mode is located at the wavelength range of the OPA laser. The crystal has a square-lattice structure, with the lattice constant and radius of the air hole being 220 nm and 90 nm, respectively. A line defect is introduced right at the center of the sample, with the width

788 | J. Mater. Chem. C, 2014, 2, 783–800

This journal is © The Royal Society of Chemistry 2014

(center-to-center distance between two adjacent rows of air holes) being 310 nm. The patterned area is about 2.5 μm × 100 μm. The transmission spectrum and time delay curve were measured, which showed that the quality factor of the defect mode is around 140, and the response time of the switching is around 10 ps, and the contrast of the "ON" and "OFF" state is about 70% (from 20% to 90%) under the pump intensity of 18.7 GW cm^{-2}. The experiment also showed that the defect mode shifts continuously when the pump intensities increased.

5. All-Optical switching in three-dimensional nonlinear photonic crystals

Due to development of state-of-the-art microfabrication technologies, good quality PC samples can be fabricated readily and most of the studies on the visible PC are focused on 2D PCs because of the relative ease of fabrication. Nonetheless, extensive efforts have also been made towards visible and infrared 3D PCs continually ever since the concept of a PC was raised. Different methods are diligently exploited to realize 3D PC structures in the infrared and visible bands.

The self-assembly method is easy to operate and is able to grow samples with a large area, so this technique has received more and more attention and many improvements have been introduced. The earlier studies of self-assembly methods include repulsive electrostatic interactions,[58–60] gravitational sedimentation,[61] electrophoresis,[62] physical limited method,[63] templating method[64] and so on. These methods were found to involve obvious disadvantages, such as long preparation time, difficulty in controlling the growth progress, bad crystalline quality, and complex preparation techniques. The vertical deposition method, first proposed by Jiang and Colvin in 1999,[65] has been proven to be successful for fabricating a high quality 3D opal PC. Since proposed, the method has received much attention, and now it has become the widely used method to fabricate 3D PCs.

Recently a new self-assembly method called the pressure controlled isothermal heating vertical deposition method (PCIHVD) was developed by Meng's group.[66] The new method is highly effective, easy to control and operate, has good repeatability and is suitable for various diameters of spheres. Using this method, a series of high quality polystyrene 3D opal PC samples have been successfully synthesized. The PCIHVD method has proven to be very suitable for preparation of high quality 3D polystyrene PC samples. Based on the PCIHVD method, we have synthesized high-quality 3D opal polystyrene NPCs with sphere diameters of 235 nm, 360 nm, 451 nm, 596 nm and 1000 nm. The SEM images of these samples are shown in Fig. 3(a)–(e). The corresponding transmission spectra are displayed in Fig. 3(f). The strong attenuation at the band gaps and the steep band gap edge clearly indicate that good periodicity and optical quality have been achieved in these samples. In addition, it is much easier to have a large area NPC sample than for 2D polymer NPCs built via nanofabrication technologies.
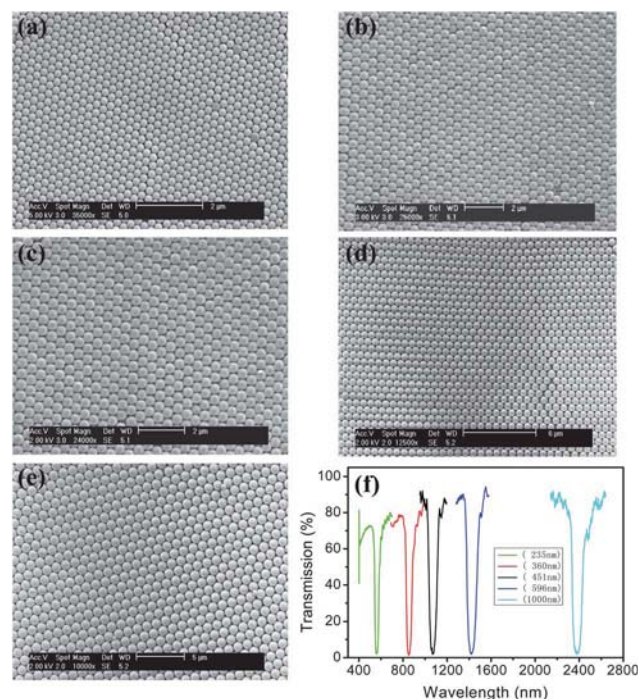
Fig. 3 Synthesis and optical characterization of polystyrene opal 3D photonic crystals synthesized by the PCIHVD method under the optimal growth conditions. Top view SEM images of the opal photonic crystal with the sphere diameter of (a) 235 nm, (b) 360 nm, (c) 451 nm, (d) 596 nm and (e) 1000 nm. (f) Measured transmission spectra for the above photonic crystals.

In the above experiment of 2D NPC optical switching, we have shown that the observable response time of the switching with comprehensive resolution is almost equal to the pump pulse duration. If the duration of the pump beam becomes shorter, the response time of switching will also become shorter. This is because that the response time of switching is determined by the slowest progress of the PC system. The response time of the polystyrene polymer material was reported to be as short as a few femtoseconds, which means that the material itself is nearly instantaneous in response to external excitation light to change its refractive index under the usual condition of light pulse duration. In order to see to what extent the above simple law of switching response time can be further scaled down to the regime of extremely short light pulse, we proceeded to design a further experiment in hope to demonstrate all-optical switching with a response time approaching the response time limit of the nonlinear material of polystyrene. The experiment was performed in 2007, and the results were published in 2009, which showed a resolved optical switching response time of about 10 fs, nearly approaching the nonlinear response limit of polystyrene material.[67]

The ultrafast laser output from a chirped-mirrors Ti:sapphire laser (Horizon-10, CAS, Beijing) with the duration of several femtoseconds was adopted in our experiment. The pulse duration and repetition rate are about 8 fs and 80 MHz, respectively. The Fourier transform spectrum as well as the

This journal is © The Royal Society of Chemistry 2014

J. Mater. Chem. C, 2014, **2**, 783–800 | **789**

interferometric autocorrelation signal of the pulse laser are shown in Fig. 4(a) and (b), respectively. The pulse laser covers a very wide spectrum range from 600 nm to 1000 nm with the center located at around 800 nm, indicating a very narrow pulse duration down to two to three laser optical cycles, namely, 6–9 femtoseconds. The autocorrelation signal is more direct to reflect the time-domain properties of the pulse laser. The curve in Fig. 4(b) has a full width at half maximum of about 8 fs, which means that the laser pulse has a duration of about 8 fs.

The 3D sample with the sphere diameter of 350 nm was prepared by the PCIHVD method under optimized synthesis

conditions that were specifically designed for this size of sphere. The SEM picture of the synthesized polystyrene opal PC sample is displayed in Fig. 4(c). The corresponding measured linear transmission spectrum is shown in Fig. 4(d). The central wavelength of the band gap is located at 800 nm. The short-wavelength band gap edge appears steeper than the long-wavelength band gap edge, so the probe beam in this experiment is selected at the wavelength of 785 nm, which is located at the short-wavelength band gap edge.

The pump-probe technique was also used to characterize all-optical switching in our 3D polystyrene opal PCs. The coupling problem in these large-area 3D PC structures is much simpler compared with the situation of 2D PCs. Our samples fabricated by the PCIHVD method have a face-centered cubic structure and their (111) plane is parallel to the surface of the substrate, namely, the Γ–L crystalline direction is perpendicular to the surface. For this reason, we often use the directional band gap of Γ–L for optical switching experiment. Only the scheme of band gap edge shift under the external pump light was considered in this system. As useful defects are difficult to deliberately introduce into the 3D PC in a controllable and accurate way, the defect mode shift scheme was not exploited for realizing all-optical switching. Although the opal PC does not have a complete band gap due to low index contrast and structural symmetry, it suffices to only consider a directional band gap for the current purpose. In this regard, the 3D PC behaves like a one dimensional PC, namely, a periodic multilayer distributed Bragg reflector. Usually the pump or probe laser can be just simply set to be normally incident upon the upper surface of the sample. However, as the pump and probe beams have the same wavelength, a small angle between the two beams is needed for splitting the beams passing through the sample. Generally, the angle is controlled within 10°.

The experimental setup is schematically illustrated in Fig. 4(e). We should point out that this experiment needs to be under very precise control in order to have comprehensive results. As both the pump and probe beams are ultrafast pulses with a duration of several femtoseconds, the synchronization will be greatly degraded and even disappear when the deflection of the optical path difference is longer than 3 μm. By precise positioning and careful tuning of the optical delay path, as well as careful control of the stability of the femtosecond laser, the time delay curve for optical switching was obtained and is depicted in Fig. 4(f). From the FWHM of the curve the response time of this all-optical switching is found to be about 10 fs, also close to the pulse duration time. The contrast of transmittance change for this optical switching is only 15% (from 35% to 50%), which is not high enough. Possible reasons for this relatively low contrast of signals include too short a pulse duration time, instability of the pulse laser, not steep enough band gap edge, and inaccuracy for determination of the delay path, and so on. It seems that the optical switching response speed for the current NPC has been close to its limit set by the finite intrinsic material response time of polystyrene.

Fig. 4 Experimental characterization of 10 fs optical switching in a 3D NPC. (a) Fourier transform spectrum and (b) corresponding interferometric autocorrelation signals of the pump pulse laser beam with 8 fs duration. (c) SEM image and (d) measured transmission spectrum of the polystyrene opal photonic crystal sample with the sphere diameter of 350 nm. The probe light at a wavelength of 785 nm (indicated by the arrow) is located at the band gap edge of the photonic crystal. (e) Experimental setup for characterization of optical switching in the 3D polystyrene photonic crystals for sub-10 fs pump and probe pulse laser. (f) Measured and (g) calculated transmittance change with respect to the time delay between pump and probe light. The wavelength of the probe light is 780 nm and the pump intensity is 20.6 GW cm^{-2}.

790 | J. Mater. Chem. C, 2014, 2, 783–800

This journal is © The Royal Society of Chemistry 2014

6. Silicon–polystyrene hybrid nonlinear photonic crystals

The realization of ultrafast all-optical switches is either based on 2D or 3D polystyrene NPCs. Although an extremely fast switching time down to 10 fs has been demonstrated in the 3D polystyrene NPC, the previously proposed NPC structures show difficulties in building integrated optical circuits or devices on a single chip. In particular, they are incompatible with overwhelmingly popular silicon photonics. A straightforward and efficient way for fabricating high-performance NPC integrated optical devices is to combine planar silicon 2D PC slab structures with polystyrene, which is schematically drawn in Fig. 5(a). The silicon–polystyrene (Si–PS) hybrid 2D NPC slab is made by infiltration of polystyrene into the air holes of the silicon 2D PC slab. It takes advantage of the high-index contrast of silicon and superior optical nonlinearity of polystyrene, and ease of integration with other silicon optical devices.[68]

The key point in fabricating this semiconductor–polymer compound NPC lies in how to uniformly and densely fill polymers into the small air holes with a diameter of only hundreds of nanometers. Previously, several techniques have been employed for the infiltration of PCs with organic composites.[46,69–74] However, specific problems, such as delamination and shrinkage of the infiltrants, have to be addressed in these technical processes. For example, solution infiltration of a PC with polymers results in shrinkage and trapped air bubbles after the removal of solvent.[70] Monomer infiltration and subsequent polymerization can lead to a good degree of infiltration, nevertheless, the materials suitable for this approach are limited and frequently they experience 10–15% of shrinkage after the thermally initiated polymerization.[72,73] Quite recently the vapor deposition method has been chosen to completely fill the silicon slot waveguide with a specific small organic

molecule, where good homogeneity originates from the assembly of an amorphous phase without the formation of microcrystals or grains.[75] So in order to homogeneously fill the hundred nanometer sized holes or slots, the above infiltration methods are all limited to certain kinds of organic molecules. A more general and practical technique for uniformly infiltrating polymer into semiconductor PC air hole arrays is highly required. So we present a feasible method to fabricate high-quality semiconductor–polymer compound NPCs by utilizing the nano-imprint lithographic (NIL) technique, which is believed to be universal for all the thermoplastic materials.[76]

The NIL technique was invented by Stephen Y. Chou in 1995 to replicate the nanostructure conveniently with the advantages of cost-effectiveness and high throughput.[77,78] For the common thermal NIL the principal procedure is as follows. A mold with nanostructures on its surface is pressed into a thin resist coated on a substrate. Keeping constant high pressure and the temperature beyond the glass transition temperature T_g of the resist, the resist becomes viscous and the flowing of it under high pressure will infiltrate the void region of the nanostructure completely after adequate time. After the removal of the mold the nanostructures are transferred into the resist film. So high-quality polymeric PC slab structures have been successfully fabricated by this technique.[79,80] NIL is usually treated only as a lithography technique for generating nano-patterns in the resist film. The great potential as an infiltration technique is largely neglected. So we envisage that if we remove the substrate instead of the mold after the imprint process, we would get perfect mold-resist compound structures.

The fabrication procedure is illustrated in Fig. 5(b). Concisely it can be divided into two parts, *i.e.* the fabrication of the PC mold on SOI structure and the preparation of the polystyrene film coated on the passivated silicon substrate. In our case silicon PC patterns were fabricated using electron-beam lithography (Raith150, Germany) combined with HBr-based inductively coupled plasma (System100, Oxford instruments, UK) etching. Then the NIL (Eitre-3, Obducat, Sweden) technique was adopted to fill the array of air holes of silicon PC slab with polystyrene for the formation of the compound NPC structure. Here it must be emphasized that stable temperature and homogeneous large-area pressure during the imprint process are the crucial conditions for the success of NIL. In our NIL system the pressure applied to the mold and substrate are offered by compressed air, which results in uniform pressure upon the whole area. Stable and program-controllable temperature is provided in the imprint chamber. Under an appropriate imprint condition of temperature, pressure, and contact time, a polystyrene film with thickness of 1–2 μm is left on top of the silicon layer. The optimal imprint conditions we found for our process were 160 °C for temperature and 50 bar for pressure with a contact time of 5 minutes beyond the T_g temperature. According to our early theoretical work,[81] as the thickness of the polystyrene layer above the semiconductor membrane is far larger than the lattice constant, the band location and band gap width of the fabricated compound NPC will reach a steady magnitude that is close to the values for the NPC with an infinitely thick polystyrene overlayer. Furthermore, as the
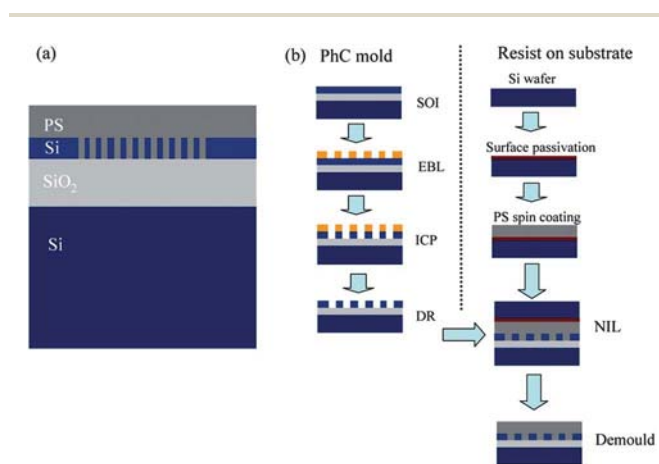
Fig. 5 Technological processing based on NIL for fabricating high-quality PS–Si hybrid NPC structures. (a) Schematics of the fabricated compound structure and (b) the fabrication procedure. The fabricated compound structure is a multilayer structure, from top to down corresponding to polystyrene layer, silicon layer with photonic crystal hole array filled with polystyrene, the silicon dioxide layer and the silicon substrate.

This journal is © The Royal Society of Chemistry 2014

J. Mater. Chem. C, 2014, **2**, 783–800 | 791

polystyrene film is thick enough, the influence of the roughness of the top surface of the polystyrene on the transmission spectrum can also be neglected.

In order to accurately characterize the effect of the infiltration, we cut the structure using FIB lithography. In this process, the 1–2 μm polystyrene thin film has been largely polished out to a very thin and rough layer (tens of nanometers thick) covering the silicon structure. Fig. 6(a) and (b) show the cross-sectional SEM view of the compound NPC slabs. The residual polystyrene gums can be clearly seen here. We can see that complete filling for all holes is achieved using this technique. The polystyrene fills the holes ideally and conformally without shrinkage and delamination from the side walls. To further clarify that the holes are undoubtedly infiltrated with polystyrene rather than an imaging error arising from the poor conductivity of polystyrene, we use a local deposition method to examine whether the holes are infiltrated or not, as is shown in Fig. 6(c) and (d). Firstly we remove the covered polystyrene layer of the compound structure totally by utilization of O_2 reactive ion etching (RIE) until the silicon surface emerges exactly. Then we locally deposit a layer of platinum (Pt) by FIB induced deposition. After that we cut the deposited region by FIB, and we can see from the cross-sectional image [Fig. 6(c)] that Pt could not deposit into the array of holes. For comparison, we deposit a Pt layer on a PC structure without polystyrene imprinted and we

can see from Fig. 6(d) that Pt can fill the air hole arrays completely. Based on the above SEM analysis results, it can be inferred that the silicon PCs are homogeneously and completely filled with polystyrene.

As we know, infiltration of silicon PCs with high index polymer, which leads to an increase of the effective refractive index, will result in the red-shift of the PBG. To optically characterize the band shift effect of the PBG by infiltration of polystyrene, the transmission spectrum is measured along the Γ–K direction of a triangular-lattice complete NPC, as is represented in Fig. 7. Optical measurements are performed with the end-face fiber coupling system.[82–84] The input optical signal with TE polarization comes from a continuous wave tunable diode laser with wavelength ranging from 1500 to 1640 nm, and launched into one facet of the silicon strip waveguide via a single-mode lensed fiber. The transmission signal is detected by a power meter via another lensed fiber collecting the emitted signal from the output side. The output strip waveguide was gradually tapered from 10 μm at the place adjacent to the NPC structure to 1.5 μm at the end face of the whole sample that connects with tapered fiber lens, so that we can collect more signal light transmitting through the NPC structures. The measured transmission spectra of the complete silicon PC structure before and after infiltration are presented in Fig. 7(c). In order to examine our measured results, we calculate the transmission spectrum for the empty and the filled PCs utilizing the 3D finite-difference time-domain (FDTD) method, which are shown in Fig. 7(d). The simulation data show an average 20 nm red-shift of the band edge after infiltration of polystyrene, which is close to the value
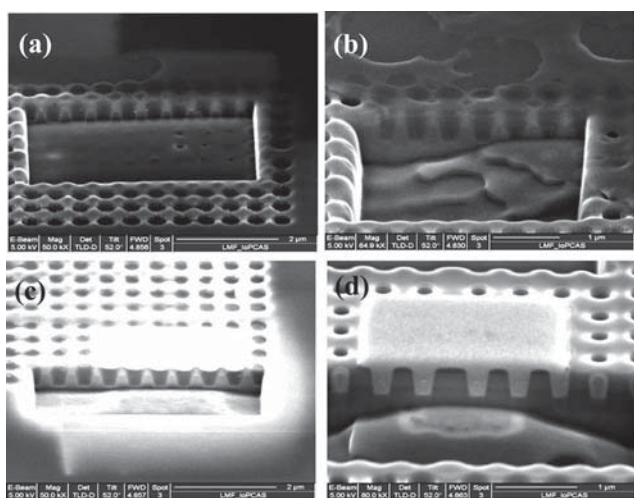
Fig. 6 Scanning electron microscopy characterization of the crystalline quality. (a) and (b) are the cross-section SEM images of the compound photonic crystal structure. The dark grey color corresponds to the polystyrene while the light grey color corresponds to the silicon owing to the difference between their conductivity. We can see that polystyrene fills the holes ideally and conformally without shrinkage and delamination from the side walls. (c) The cross-section SEM image of the compound photonic crystal structure after the deposition of Pt layer. We deposit a layer of Pt by FIB induced deposition on the surface of the compound structure after taking out the surface polymer by the O_2 reactive-ion-etching, and we can see that Pt cannot deposit into the holes of the array, indicating complete infiltration of polystyrene into the air holes. (d) The cross-section SEM image of the non-infiltrated photonic crystal structure after the deposition of Pt layer. In contrast with panel (c), we can see that the Pt can deposit into the air holes and reach their bottom. The bright rectangular bump on top of the slab is the deposited Pt layer.
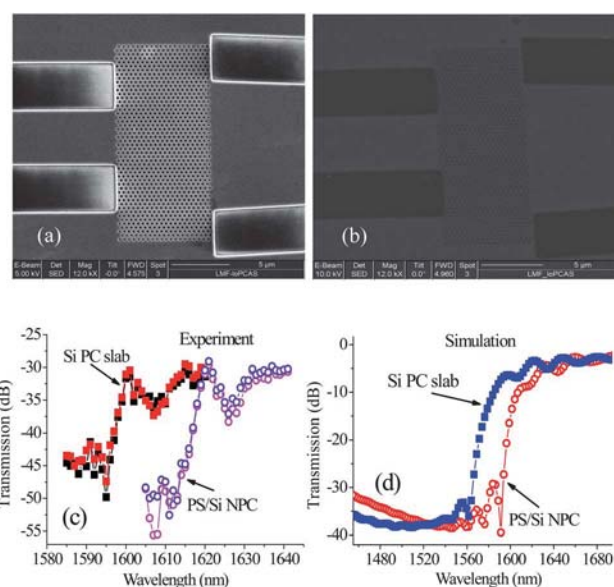
Fig. 7 Optical characterization of the crystalline quality of the fabricated PS−Si hybrid NPCs. (a) SEM top view pictures of a triangular-lattice complete photonic crystal before infiltration and (b) SEM top view pictures after infiltration by utilizing NIL technique. (c) Experimental transmission spectra of the TE-like mode along the Γ−K direction of the empty and infiltrated triangular-lattice PCs. (d) 3D-FDTD simulation results of the empty and infiltrated triangular-lattice PCs.

792 | J. Mater. Chem. C, 2014, 2, 783–800

This journal is © The Royal Society of Chemistry 2014

found in experiments. The significant shift of the band-edge and large transmission contrast indicate that the filling of the PC holes is complete and uniform. The absolute position and the line shape (*e.g.*, the steepness) of the band edge show a slight deviation between experiment and simulation, and this can be attributed to the nanofabrication imprecision as well as the departure of the models used in the numerical simulation from the practical samples under experimental studies. For instance, the input and output ridge waveguides have been neglected in the numerical simulations for the sake of simplicity.

In addition to the complete compound NPC, we have also successfully built a compound NPC microcavity following the same fabrication procedure to further verify the validity of this NIL method. The SEM pictures of the PC microcavity before and after infiltration of polystyrene are presented in Fig. 8(a) and (b). Because the microcavity is directly coupled to the input and output waveguide, the position of transmission peaks of the resonant frequency between the optical measurement and the 3D FDTD simulation are quite close. More importantly, the values of *Q*-factor for both PC and NPC cavity modes are also close. All these optical properties strongly indicate that the compound structures are of high-quality, which will place a solid material basis for further exploring ultrafast optical switching and logic devices on the platform of these Si–PS hybrid NPC structures.

7. Air-bridged low-index polystyrene NPC slab

Although highly nonlinear polymer or nanocomposite polymer materials can outperform semiconductor materials in terms of
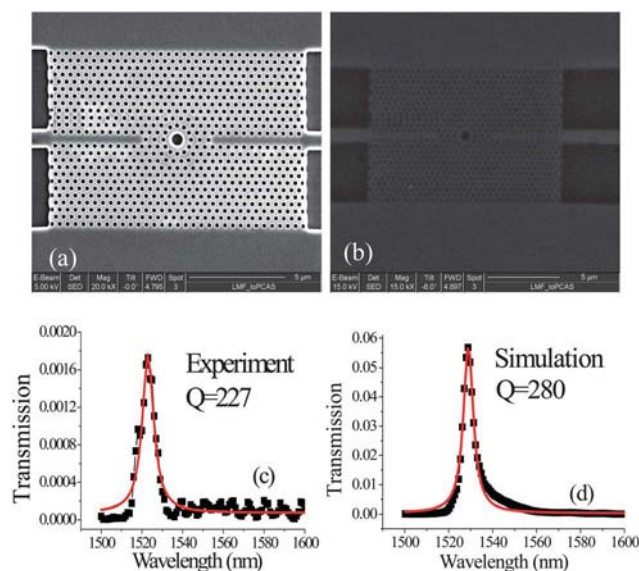
Fig. 8 Optical characterization of the fabrication quality of PS−Si hybrid NPC cavities. (a) SEM top view pictures of a PC microcavity before infiltration and (b) SEM top view pictures after infiltration by utilizing NIL technique. (c) Experimental transmission spectra of the compound PC microcavity. (d) 3D-FDTD simulation results of the compound PC microcavity. The red line is the fitting line with Lorentzian line-shape.

large Kerr coefficient and ultrafast response speed,[85–88] the success of nonlinear optical devices strongly depends on the success in fabricating these complicated devices. In Section 4 we have discussed fabrication of a 2D polystyrene NPC. As the polystyrene thin film is deposited on glass substrate, light tends to leak into the glass substrate when it transports along the 2D NPC, due to the small refractive index contrast between polystyrene and glass and consequently weak confinement of light within the NPC. The best confinement of light is achieved *via* a so-called air-bridged 2D NPC slab, where the 2D band gap confines light in the parallel plane of the slab and the total internal reflection confines light within the slab. Although this technique is pretty mature for silicon PC,[82–84] the appropriate technique for fabricating polymeric 2D NPC slab structures is still in its initial stage. Early 2D polymeric PC slab structures were built by the direct electron-beam lithography technique. However, this technique is inevitably restricted to electron-beam sensitive polymers.[89] Subsequently a high-quality 2D polymeric NPC slab is proposed to be fabricated by combining electron-beam lithography with reactive ion etching.[90] Furthermore, NIL and wet chemical etching are used to fabricate air-suspended 2D polystyrene PC slab waveguides.[91] Nevertheless, the above fabrication methods involve multiple processing steps such as lithography and ion etching, which leads to a great deal of time consumption. In Section 4 we have presented that not only 2D polymeric NPC but also 2D polymeric NPC microcavities can be successfully constructed by using FIB milling.[11,92] Recently, we successfully used this technique to fabricate an air-bridged 2D polymetric NPC slab, which has a similar geometric configuration to the usual air-bridged silicon 2D PC slab.[93]

In the process of FIB etching, air hole arrays are directly drilled into the polymeric thin film by the heavy ion bombardment, such as Ga^+ ions, so that no mask or mold is needed in advance. Previously our 2D polymeric PC slab structures were all laid on a relatively low refractive index substrate materials such as silica. Hence the small refractive index contrast between polymer slab and silica substrate is unsuitable to achieve high-*Q* microcavities, which largely limits the potential application of highly nonlinear polymer materials. So it is meaningful to explore an appropriate fabrication method for achieving air-bridged polymeric PC slab structures. On the basis of FIB milling, we combine the wet chemical etching method to fabricate high-quality air-bridged polystyrene 2D NPC slabs. As illustrated in Fig. 9, the air-bridged 2D NPC slab structures offer the best possible refractive index contrast between polystyrene and air, and thus the best PBG effects.

The polymer we studied is the polystyrene material with a normal molecular weight of 8 000 000 (Fluka Chemie Company, Switzerland). The fabrication procedure is schematically illustrated in Fig. 10. It can be concisely described as follows. Firstly, the substrate is prepared by depositing a thick silica layer (with thickness about 1 μm) on the silicon surface using plasma-enhanced chemical vapor deposition (PECVD), where the silica membrane is chosen as the sacrificial layer to form the air-bridged structure. Secondly, the polystyrene layer

This journal is © The Royal Society of Chemistry 2014

J. Mater. Chem. C, 2014, **2**, 783–800 | 793
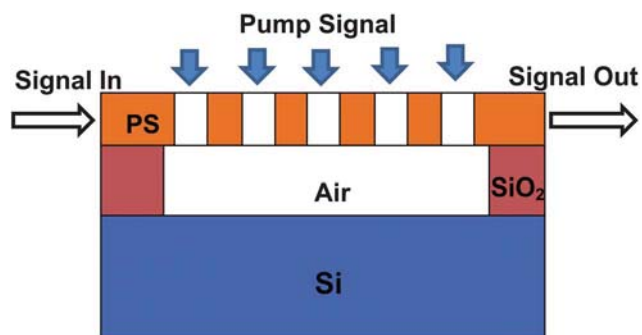
Fig. 9 Schematics of optical switching in polystyrene (PS) air-bridged 2D NPC slabs. The NPC is made by milling air holes into the polystyrene membrane and supports confined Bloch's modes within the membrane due to the refractive index contrast between air and polystyrene.
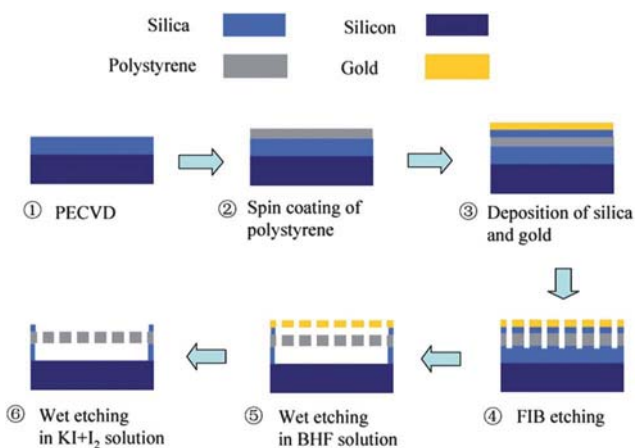
Fig. 10 Schematic illustration of the fabrication procedure for polystyrene air-bridged 2D NPC slab.

is put on top of the silica layer by spin coating. By adjusting the rotation time and speed we can control the thickness of the polystyrene layer. In order to obtain good optical confinement in the vertical direction and maintain a single-mode, the thickness for the polystyrene slab is fixed as 1 to 1.5a, where a represents the lattice constant of the PC pattern. Setting the PBG in the near-infrared region, the thickness of the polystyrene slab is controlled in the range of 500 to 800 nm. Before FIB etching, two layers of silica and gold with thicknesses of 50 nm and 100 nm are deposited on top of the polystyrene slab. The usage of gold layer is for the charge removal during the FIB etching process and the silica layer is of help to completely get rid of the gold layer in the final wet chemical etching step. The FIB system is employed to prepare the periodical patterns in the polystyrene layer. Simultaneously considering the fabrication time and precision, an appropriate spot current of 100 pA is used to drill the air hole arrays, where the cylindrical air holes cut through the polystyrene layer down to the silica substrate. To form the air suspended PC slab, the samples are then immersed into buffered hydrofluoric acid (BHF) to etch the

underlying silica layer. The immersion time is precisely controlled to fully remove the silica layer underneath the hole arrays. Finally the top gold layer is removed by dipping the sample into a KI and I_2 mixed solution.

The SEM images of several typical fabricated samples are presented in Fig. 11. For the sake of obtaining clear and stable SEM pictures the upmost gold layer is reserved. Not only the conventional 2D air-bridged polystyrene PC slab but also the 1D nanobeam structures have been successfully fabricated. From Fig. 11 it can be seen that the fabricated air hole arrays are uniform and homogeneous. The hole diameters marked in Fig. 11(b) and (e) are approximately 330 nm and 430 nm for the 1D nanobeam structures and 2D triangular lattice PC, respectively. Taking into account the aspect ratio between slab thickness and hole diameter approaching 2 : 1, it is unavoidable that the designed cylindrical hole tends to become a little cone shaped in practical samples. In addition, an obvious air gap with thickness near 1 μm can be seen in Fig. 11(c) and (f), when the samples are tilted at an angle of 52°.
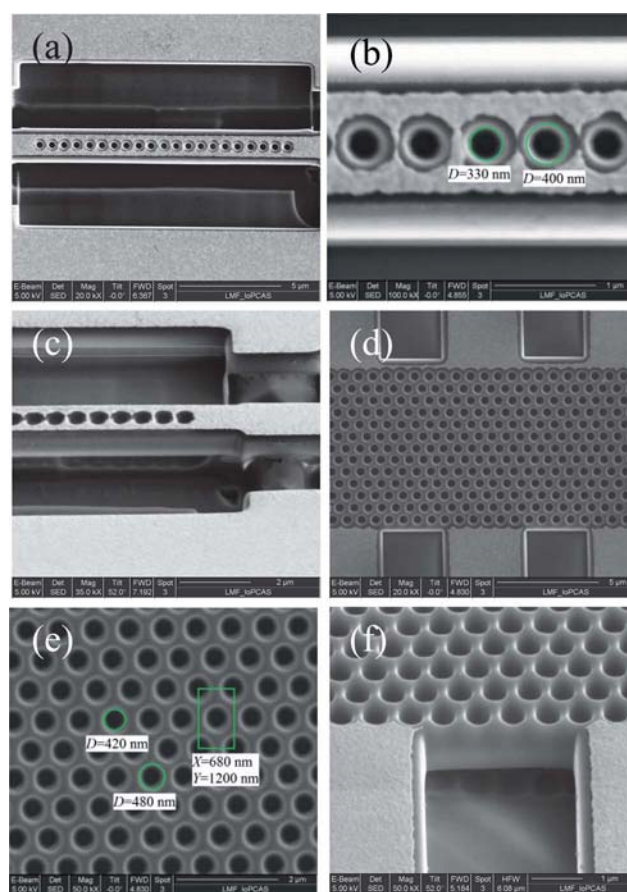
Fig. 11 SEM images of the fabricated samples. (a)–(c) SEM images of the 1D air-bridged PS nanobeam structures. (d)–(f) SEM images of the 2D air-bridged PS slab structures. The diameters of the fabricated holes and the lattice constant of the PC structures are marked in (b) and (e). The designed cylindrical hole tends to become a little cone shaped in practical samples. In Fig. 11c and f the samples are tilted at an angle of 52°. For the sake of obtaining clear and stable SEM images, the upmost gold layer is not removed.

794 | J. Mater. Chem. C, 2014, 2, 783–800

This journal is © The Royal Society of Chemistry 2014

8. Logic devices

In recent years, all-optical logic gates, which can fulfil various logical function operations, have received much attention for their potential applications in ultrafast information processing,[94,95] all-optical computing systems,[96,97] and so on. There are several methods to realize all-optical logic functions, such as semiconductor optical amplifier,[98] optical interference effect,[99,100] and third-order nonlinear effect.[101–103] Nowadays, all-optical logic gates based on the third-order nonlinear effect of PC structures have received increasing attention. When considering their practical applications, ultra-compact all-optical logic gates realized in 2D PC slabs show more prospective.[104] Such 2D PC slabs provide confinement of light in the vertical direction by total internal reflection and allow control of light with the PC in the plane of the slab. When the substrate material underneath the 2D PC slabs is removed, the so-called air-bridged PC slab can be formed, which can provide tighter confinement in the vertical directional so as to achieve a high quality factor microcavity in the low-index polymer materials. This type of PC has great potentiality as ultra-compact integrated optical devices compared to the 3D PC. Optical logic gates, similar to optical switches, must address the key issues of ultrafast response speed, low pump power and high signal contrast. NPC slabs made from polymer materials or Ag–polymer hybrid materials can be good solutions.

Our logic gates are based on the two-path and two-cavity configuration,[104] which is illustrated in Fig. 12. For realizing various logic functions, this structure contains two cavities. The input signal light is divided into two paths by an input Y-type waveguide, and then interacts with the two cavities. The PC slab is air-suspended in this situation. The air-bridged 2D PC film formed by etching a periodical square lattice of air holes is adopted. The radius of the air holes is $0.25a$, where a is the lattice constant. The thickness of this slab is $1.5a$. Finally, they are coupled together to an output Y-type waveguide. At the same time, two pump lights I_1 and I_2 are incident onto the upper surface of the PC structure normally. In our designs here, the input signal is a continuous wave with the power of 0.5 kW cm^{-2}, while the pump lights are picosecond ultrashort pulses whose average pulse powers are in the order of 10 MW cm^{-2}. Considering the experimental conditions that the area of NPC structures is less than 400 μm^2 and the focus radius of pump light is
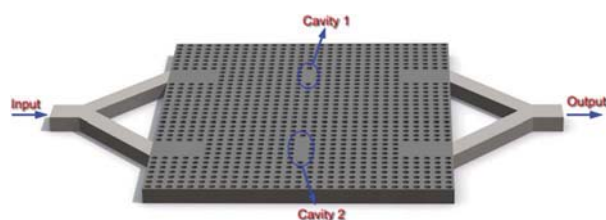
Fig. 12 The schematic illustration of logic gates based on the two-path two-cavity configuration built on a polystyrene 2D NPC slab.

about 10 μm, both of the pump lights will interact with the two cavities.

In order to satisfy the ultrafast response speed, low pump power and high signal contrast, a relatively high-Q microcavity must be properly designed with the highly nonlinear polymer materials. The compound Ag–polymer film is chosen as our nonlinear material, whose linear refractive index is 1.59 and third-order nonlinear susceptibility is set at 1.0×10^{-7} esu. The polymer is polystyrene, which has a large third-order nonlinearity and ultrafast nonlinear optical response speed down to several femtoseconds. Due to the low refractive index of polystyrene materials, the line defect cavity configuration is chosen to realize a high-Q microcavity, where the line defect is formed by removing the center seven air holes along the y-axis. After fine tuning the air holes near the defect region, the quality factor can be improved to the order of 10^3, which can be seen in Fig. 13.

In our case, the third-order nonlinear susceptibility of Ag–polymer film is set at 1.0×10^{-7} esu, so with the pump light, the refractive index will increase and the defect mode will shift to lower frequency. Fig. 13(e) shows the shift of the defect mode of a L7-type cavity with and without the pump light, where the "Lm" cavity corresponds to a cavity whose length along the y-axis is m times the lattice constant. When the pump power is 45 MW cm^{-2}, the normalized resonant frequency of the defect mode shifts from 0.38008 to 0.37932 ($2\pi c/a$). If the lattice constant is $a = 590$ nm, the corresponding wavelength shifts from 1552.3 nm to 1555.4 nm. Due to the relatively high quality factor of this cavity ($Q = 1558$), the spectral width of the defect mode is very narrow (about 1 nm), which makes a high transmission contrast with and without pump light. So by precisely controlling the intensity of the pump light, the transmission of the input signal can be switched from "ON" to "OFF" or *vice versa*. This is the foundation of operation of our logic gates based on the shift of the resonant frequency of the cavity. By suitable selection of the resonant frequencies of these two cavities, we can realize all-optical logic gates with different logic functions. Here, at each path, the distance between the input or output waveguide and the cavity is $16a$, and the existence of waveguides will not influence the properties of the cavity mode. The frequency of the input probe light is denoted as f_0, while the resonant frequencies of the two cavities are f_1 and f_2, respectively. Table 1 shows the principles of all-optical AND, NAND, OR, and NOR gates, respectively.

We take the AND gate as an example to introduce the principle of our logic operation. For the AND gate, both of the two cavities are selected as the L7-type cavity, whose quality factor is about 1558, and the normalized resonant frequency is $f_1 = f_2 = 0.38008$. The normalized frequency of the input signal light is set at $f_0 = 0.37932$. At first, due to the frequency deflection between the input signal light and the cavity mode, the signal light is localized at the forbidden gap, and its transmission is as low as 1.9%. With the incidence of single pump light I_1 or I_2, the refractive index of Ag–polymer increases, and the resonant frequency of the cavity will shift to lower frequency. When the pump power is 22.5 MW cm^{-2}, which makes the refractive index

This journal is © The Royal Society of Chemistry 2014

J. Mater. Chem. C, 2014, **2**, 783–800 | **795**
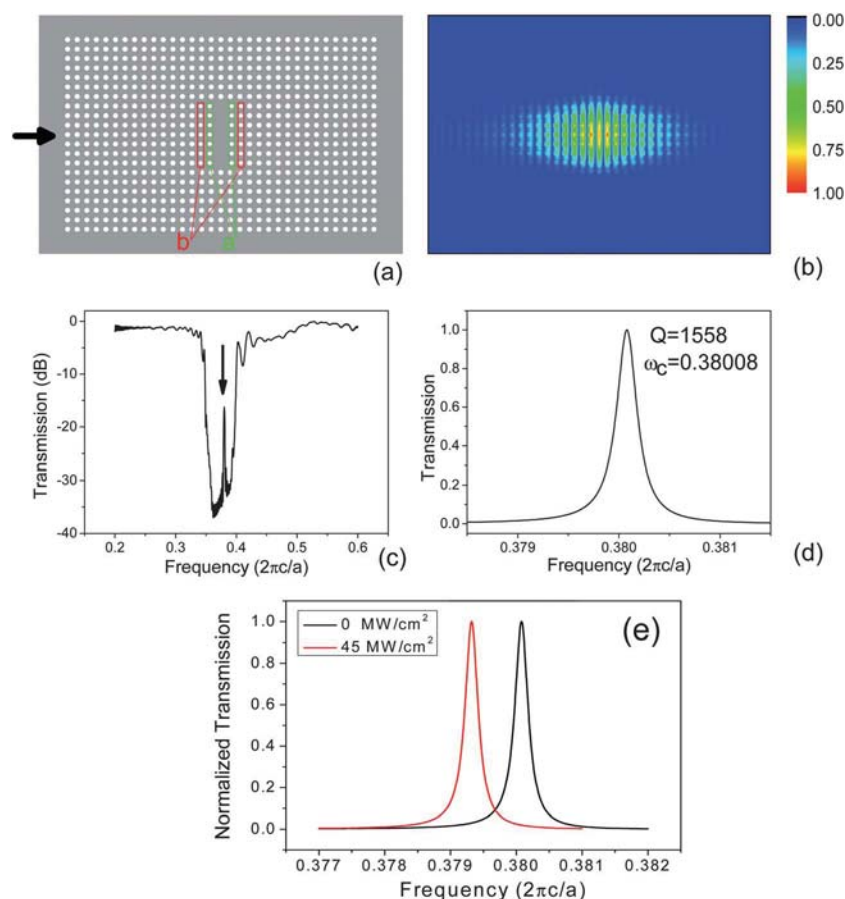
Fig. 13 Optical switching based on 2D NPC slab cavities. (a) The schematic structure of optimized NPC cavity. (b) The electric field distribution at the resonant frequency of the optimized NPC cavity. (c) The calculated transmission spectrum. (d) The optimized cavity mode. The normalized resonant frequency is 0.38008, and the quality factor is 1558. (e) The shift of defect mode under pump light. The black line corresponds to the linear case, and the red line represents the nonlinear case with the pump power of 45 MW cm^{-2}. The transmission is normalized to its peak value.

change by 0.2%, the nonlinear resonant frequency shifts to 0.3797. In this case, although the frequency deflection between the input signal light and the cavity mode becomes less, due to the narrow spectral width, the transmission is still low, which is about 9.5%. Under the excitation of both pump lights I_1 and I_2, the frequency of defect mode shifts to the frequency of the input signal light exactly, and the transmission reaches up to 100%. Table 2 shows the truth table of the AND gate. Similar to the AND gate, the NAND, OR and NOR gate can be realized in such a manner through carefully selecting the frequency of the probe light, the resonant frequency of the two cavities and the intensity of the pump light.[104]

As has been explicitly discussed in Sections 6 and 7, we can fabricate high-quality silicon–polystyrene compound PC slabs and air-bridged polystyrene PC slabs. Following the same fabrication procedure we have already built the two-path and two-cavity logic gates based on the Si–PS compound NPC and polystyrene NPC slab. The SEM pictures of two typical fabricated logic devices are presented in Fig. 14, where the sample quality can be clearly seen. Although the optical measurements of the logic gates are still ongoing, our logic gates scheme indicates the superiority of possessing ultrafast response speed, low pump power and high signal contrast.

Table 1 The principles of all-optical AND, NAND, OR, and NOR gates

Logic gate	Initialization	I_1	I_2	I_1 & I_2
AND ($f_1 = f_2$)	$f_1 \neq f_0$ logic 0	$f_1 \neq f_0$ logic 0	$f_1 \neq f_0$ logic 0	$f_1 = f_0$ logic 1
NAND ($f_1 \neq f_2$)	$f_2 = f_0$ logic 1	$f_1 = f_0$ logic 1	$f_1 = f_0$ logic 1	$f_1 \neq f_0, f_2 \neq f_0$ logic 0
OR ($f_1 \neq f_2$)	$f_1 \neq f_0, f_2 \neq f_0$ logic 0	$f_2 = f_0$ logic 1	$f_2 = f_0$ logic 1	$f_1 = f_0$ logic 1
NOR ($f_1 = f_2$)	$f_1 = f_0$ logic 1	$f_1 \neq f_0$ logic 0	$f_1 \neq f_0$ logic 0	$f_1 \neq f_0$ logic 0

Table 2 Truth table of the AND gate

Pump 1		Pump 2		Output	
Power (MW cm^{-2})	Logic level	Power (MW cm^{-2})	Logic level	Transmission (%)	Logic level
0	0	0	0	1.9	0
22.5	1	0	0	9.5	0
0	0	22.5	1	9.5	0
22.5	1	22.5	1	100	1
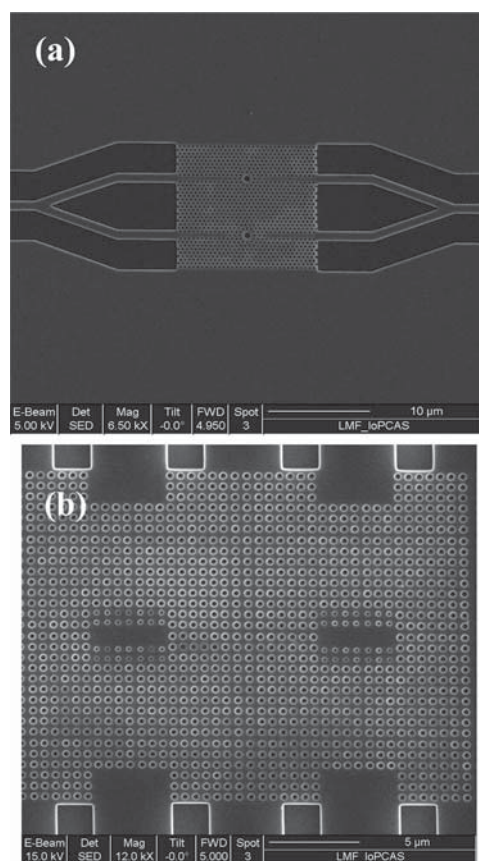
Fig. 14 Fabrication of NPC logic gate devices. (a) SEM of a two-path two-cavity PS–Si compound NPC logic gate. (b) SEM of a two-path two-cavity polystyrene air-bridged 2D NPC slab logic gate.

9. Summary and perspective

In this feature article we have briefly described our recent experimental progress on exploring ultrafast all-optical switching in 2D and 3D polystyrene Kerr NPCs and our efforts to continually improve the switching speed to the realm of a few femtoseconds. We have introduced different mechanisms for realization of all-optical switching and discussed approaches to prepare high-quality NPC samples with considerable band gap attenuation and steep band gap edge by means of micro-fabrication technique and self-assembly technique. We have described the femtosecond pump-probe technique that is used to characterize the overall performance characteristics of all-optical switching such as the response speed, switching signal contrast, and pump power threshold. The development of state-of-the-art ultrafast pulse laser technique enables us to experimentally explore the ultimate response speed limit and underlying dynamical picture of all-optical switching based on the polystyrene polymer material. The response time has been scaled down continually from 10 ps, 120 fs, 20 fs, and finally to 10 fs. It seems that the response time is approximately equal to the duration time of pump laser pulse, but a few femtoseconds might have been the limit because it has already been approaching the material response time of polystyrene.

To bring ultrafast all-optical switching into reality to facilitate practical applications in optical information processing, several key issues must be addressed and solved. The first issue is to fabricate high-quality NPC structures and devices. A series of nanofabrication, material synthesis and assembly technologies need to be explored and exploited. The present review paper is mainly focused on this issue of NPC sample preparation. We have explored various nanofabrication and self-assembly technologies and successfully prepared a wide variety of NPC structures and devices. These include 2D polystyrene NPCs, 3D opal polystyrene NPCs, 2D Si–PS hybrid NPC slab, 2D polystyrene NPC slab, and nonlinear optical devices such as cavities, waveguides, and logic gates built on these platforms. Through continuous efforts, we have made great progress towards building high-quality NPC devices.

Another key issue is the ultrafast speed of optical switching and logic devices, which has been fully addressed in this paper. In bulk 2D and 3D NPC materials, down to several tens of femtoseconds optical switching has been successfully demonstrated. However, the optical performance of integrated NPC devices, such as waveguides, cavities, and logic gates built on 2D polystyrene NPC or Si–PS hybrid NPC slab has not been experimentally characterized, mainly due to the limitation of the ultrafast pump-probe technique for nanoscale devices. The measurement system must be able to resolve ultrafast (down to tens of femtoseconds), ultralow pump power (due to the low coupling efficiency of external power into nanoscale devices), and ultracompact device size (in the order of several wavelengths). We are currently trying hard to set up such a measurement system.

The final key issue is to lower the pump power in order for these NPC optical switching and logic devices to have practical meanings. This issue is not addressed in this paper. Realistically, the pump power must be significantly lowered by several

This journal is © The Royal Society of Chemistry 2014

J. Mater. Chem. C, 2014, **2**, 783–800 | **797**

orders of magnitude from the current value. In the past years, we have discussed different schemes to reduce the pump power threshold of optical switching in NPCs, such as resonant cavity effect[105–110] and surface plasmon resonance effect.[111,112] The principle is simple: enlarging the effective Kerr nonlinear response either by looking for good materials with larger Kerr nonlinear susceptibility in microscopic molecules, or by enhancing the intensity of local field exerting on Kerr nonlinear materials, or by increasing the effective interaction path of light with Kerr nonlinear materials.

These studies have taught us a lot about the fundamental principles and necessary technologies towards realization of useful ultrafast all-optical switching and logic devices in the microscale and nanoscale that can be placed into future all-optical integrated chips, where all-optical switching with high contrast, low pump power, and ultrafast speed is the ultimate goal. Although great progress has been made, there is still a long way to go. Final success should strongly rely on joint efforts from different aspects of science and technology: physics for a better working principle, optics for better detection and characterization techniques, chemistry and materials science for exploration and preparation of new better Kerr nonlinear materials, and nanotechnology for easy and accurate building of nanoscale and microscale optical switching and logic devices. As all-optical switching and logic devices are essential components in all-optical networks, the dream for large-scale optical integrated networks and their connection with traditional microelectronic integrated chips that are promising for revolutionary information processing technology will not come true without the success of bringing user friendly, easy to control and tiny all-optical switching and logic devices into reality.

Acknowledgements

References

1 S. R. Friberg, Y. Silberberg, M. K. Oliver, M. J. Andrejco, M. A. Saifi and P. W. Smith, *Appl. Phys. Lett.*, 1987, **51**, 1135.

2 V. R. Almeida, C. A. Barrios, R. R. Panepucci and M. Lipson, *Nature*, 2004, **431**, 1081–1084.

3 V. R. Almeida and M. Lipson, *Opt. Lett.*, 2004, **29**, 2387.

4 K. Sasaki and T. Nagamura, *J. Appl. Phys.*, 1998, **83**, 2894.

5 K. Sasaki and T. Nagamura, *Appl. Phys. Lett.*, 1997, **71**, 434.

6 E. Yablonovitch, *Phys. Rev. Lett.*, 1987, **58**, 2059.

7 S. John, *Phys. Rev. Lett.*, 1987, **58**, 2486.

8 M. F. Yanik, S. H. Fan and M. Soljacic, *Appl. Phys. Lett.*, 2003, **83**, 2739.

9 M. Soljacic, E. Lidorikis, J. D. Joannopoulos and L. V. Hau, *Appl. Phys. Lett.*, 2005, **86**, 171101.

10 T. Tanabe, M. Notomi, S. Mitsugi, A. Shinya and E. Kuramochi, *Appl. Phys. Lett.*, 2005, **87**, 151112.

11 X. Y. Hu, P. Jiang, C. Y. Ding, H. Yang and Q. H. Gong, *Nat. Photonics*, 2008, **2**, 185.

12 K. Nozaki, T. Tanabe, A. Shinya, S. Matsuo, T. Sato, H. Taniyama and M. Notomi, *Nat. Photonics*, 2010, **4**, 477.

13 J. L. Bredas, C. Adant, P. Tackx, A. Persoons and B. M. Pierce, *Chem. Rev.*, 1994, **94**, 243.

14 A. K. Kar, *Polym. Adv. Technol.*, 2000, **11**, 553.

15 Z. H. Jin, Z. Y. Li, K. Kasatani and H. Okamoto, *J. Lumin.*, 2007, **122**, 427.

16 P. Sharma, S. Roy and C. P. Singh, *Thin Solid Films*, 2005, **477**, 42.

17 V. Morandi, F. Marabelli, V. Amendola, M. Meneghetti and D. Comoretto, *Adv. Funct. Mater.*, 2007, **17**, 2779.

18 R. B. Boyd, *Nonlinear Optics*, Academic Press, Amsterdam, 2003.

19 M. Scalora, J. P. Dowling, C. M. Bowden and M. J. Bloemer, *Phys. Rev. Lett.*, 1994, **73**, 1368.

20 P. Tran, *Opt. Lett.*, 1996, **21**, 1138.

21 P. Tran, *Phys. Rev. B: Condens. Matter*, 1995, **52**, 10673.

22 L. X. Chen and D. Kim, *Opt. Commun.*, 2003, **218**, 19.

23 T. Hattori, N. Tsurumachi and H. Nakatsuka, *J. Opt. Soc. Am. B*, 1997, **14**, 348.

24 F. Monifi, M. Djavid, A. Ghaffari and M. S. Abrishamian, *J. Opt. Soc. Am. B*, 2008, **25**, 1805.

25 E. Centeno and D. Felbacq, *Phys. Rev. B: Condens. Matter*, 2000, **62**, R7683.

26 I. L. Lyubchanskii, N. N. Dadoenkova, A. E. Zabolotin, Y. P. Lee and T. Rasing, *J. Appl. Phys.*, 2008, **103**, 07B321.

27 S. F. Mingaleev, A. E. Miroshnichenko and Y. S. Kivshar, *Opt. Express*, 2007, **15**, 12380.

28 M. Notomi, A. Shinya, S. Mitsugi, G. Kira, E. Kuramochi and T. Tanabe, *Opt. Express*, 2005, **13**, 2678.

29 T. Tanabe, M. Notomi, S. Mitsugi, A. Shinya and E. Kuramochi, *Opt. Lett.*, 2005, **30**, 2575.

30 A. M. Yacomotti, F. Raineri, G. Vecchi, P. Monnier, R. Raj, A. Levenson, B. Ben Bakir, C. Seassal, X. Letartre, R. Viktorovitch, L. Di Cioccio and J. M. Fedeli, *Appl. Phys. Lett.*, 2006, **88**, 231107.

31 H. B. Sun, S. Matsuo and H. Misawa, *Appl. Phys. Lett.*, 1999, **74**, 786.

32 G. H. Ma, S. H. Tang, J. Shen, Z. J. Zhang and Z. Y. Hua, *Opt. Lett.*, 2004, **29**, 1769.

33 S. A. Pruzinsky and P. V. Braun, *Adv. Funct. Mater.*, 2005, **15**, 1995.

34 I. S. Maksymov, L. F. Marsal and J. Pallares, *Opt. Commun.*, 2007, **269**, 137.

35 N. Tetreault, H. Miguez and G. A. Ozin, *Adv. Mater.*, 2004, **16**, 1471.

36 A. Hache and M. Bourgeois, *Appl. Phys. Lett.*, 2000, **77**, 4089.

37 T. G. Euser, H. Wei, J. Kalkman, Y. Jun, A. Polman, D. J. Norris and W. L. Vos, *J. Appl. Phys.*, 2007, **102**, 053111.

798 | *J. Mater. Chem. C*, 2014, **2**, 783–800

This journal is © The Royal Society of Chemistry 2014

38 C. Bosshard, R. Spreiter, M. Zgonik and P. Günter, *Phys. Rev. Lett.*, 1995, **74**, 2816.

39 A. Figotin, Y. A. Godin and I. Vitebsky, *Phys. Rev. B: Condens. Matter*, 1998, **57**, 2841.

40 X. Y. Hu, Y. Q. Wang, Y. H. Liu, B. Y. Cheng and D. Z. Zhang, *Opt. Commun.*, 2004, **237**, 371.

41 I. S. Nefedov and V. N. Gusyatnikov, *J. Opt.*, 2000, **2**, 344.

42 H. S. Djie, T. Mei, J. Arokiaraj and D. Nie, *J. Appl. Phys.*, 2004, **96**, 3282.

43 F. Z. Henari, K. Morgenstern, W. J. Blau, V. A. Karavanskii and V. S. Dneprovskii, *Appl. Phys. Lett.*, 1995, **67**, 323.

44 Y. Vlasov, W. M. J. Green and F. Xia, *Nat. Photonics*, 2008, **2**, 242.

45 T. Tanabe, K. Nishiguchi, A. Shinya, E. Kuramochi, H. Inokawa, M. Notomi, K. Yamada, T. Tsuchizawa, T. Watanabe, H. Fukuda, H. Shinojima and S. Itabashi, *Appl. Phys. Lett.*, 2007, **90**, 031115.

46 S. W. Leonard, J. P. Mondia, H. M. van Driel, O. Toader, S. John, K. Busch, A. Birner, U. Gosele and V. Lehmann, *Phys. Rev. B: Condens. Matter*, 2000, **61**, R2389.

47 K. Busch and S. John, *Phys. Rev. Lett.*, 1999, **83**, 967.

48 X. Y. Hu, Y. H. Liu, J. Tian, B. Y. Cheng and D. Z. Zhang, *Appl. Phys. Lett.*, 2005, **86**, 121102.

49 Y. H. Liu, X. Y. Hu, D. X. Zhang, B. Y. Cheng, D. Z. Zhang and Q. B. Meng, *Appl. Phys. Lett.*, 2005, **86**, 151102.

50 Z. L. S. K. F. MacDonald, M. I. Stockman and N. I. Zheludev, *Nat. Photonics*, 2009, **3**, 55.

51 K. Asakawa, Y. Sugimoto, Y. Watanabe, N. Ozaki, A. Mizutani, Y. Takata, Y. Kitagawa, H. Ishikawa, N. Ikeda, K. Awazu, X. M. Wang, A. Watanabe, S. Nakamura, S. Ohkouchi, K. Inoue, M. Kristensen, O. Sigmund, P. I. Borel and R. Baets, *New J. Phys.*, 2006, **8**, 25687.

52 X. Y. Hu, Q. Zhang, Y. H. Liu, B. Y. Cheng and D. Z. Zhang, *Appl. Phys. Lett.*, 2003, **83**, 2518.

53 X. Y. Hu, Q. H. Gong, Y. H. Liu, B. Y. Cheng and D. Z. Zhang, *Appl. Phys. Lett.*, 2005, **87**, 231111.

54 D. Z. Zhang, Y. H. Liu, J. Tian, S. Feng, D. X. Zhang and B. Y. Cheng, *Proc. SPIE*, 2006, **6353**, 635307.

55 W. W. Flack, D. S. Soong, A. T. Bell and D. W. Hess, *J. Appl. Phys.*, 1984, **56**, 1199.

56 F. C. Peiris, S. Lee, U. Bindley and J. K. Furdyna, *J. Appl. Phys.*, 1998, **84**, 5194.

57 P. K. Tien, R. Ulrich and R. J. Martin, *Appl. Phys. Lett.*, 1969, **14**, 291.

58 P. Pieranski, L. Strzelecki and B. Pansu, *Phys. Rev. Lett.*, 1983, **50**, 900.

59 E. A. Kamenetzky, L. G. Magliocco and H. P. Panzer, *Science*, 1994, **263**, 207.

60 Y. N. Xia, B. Gates, Y. D. Yin and Y. Lu, *Adv. Mater.*, 2000, **12**, 693.

61 J. X. Zhu, M. Li, R. Rogers, W. Meyer, R. H. Ottewill, W. B. Russell and P. M. Chaikin, *Nature*, 1997, **387**, 883.

62 R. C. Hayward, D. A. Saville and I. A. Aksay, *Nature*, 2000, **404**, 56.

63 S. H. Park and Y. N. Xia, *Langmuir*, 1999, **15**, 266.

64 A. vanBlaaderen, R. Ruel and P. Wiltzius, *Nature*, 1997, **385**, 321.

65 P. Jiang, J. F. Bertone, K. S. Hwang and V. L. Colvin, *Chem. Mater.*, 1999, **11**, 2132.

66 Z. Y. Zheng, X. Z. Liu, Y. H. Luo, B. Y. Cheng, D. Z. Zhang, Q. B. Meng and Y. R. Wang, *Appl. Phys. Lett.*, 2007, **90**, 051910.

67 Y. Liu, F. Qin, Z. Y. Wei, Q. B. Meng, D. Z. Zhang and Z. Y. Li, *Appl. Phys. Lett.*, 2009, **95**, 131116.

68 F. Qin, Y. Liu and Z. Y. Li, *J. Opt.*, 2010, **12**, 035209.

69 P. A. El-Kallassi, S. Balog, R. Houdre, L. Balet, L. Li, M. Francardi, A. Gerardino, A. Fiore, R. Ferrini and L. Zuppirolil, *J. Opt. Soc. Am. B*, 2008, **25**, 1562.

70 J. Martz, R. Ferrini, F. Nuesch, L. Zuppiroli, B. Wild, L. A. Dunbar, R. Houdre, M. Mulot and S. Anand, *J. Appl. Phys.*, 2006, **99**, 103105.

71 S. F. Mingaleev, M. Schillinger, D. Hermann and K. Busch, *Opt. Lett.*, 2004, **29**, 2858.

72 S. Tay, J. Thomas, B. Momeni, M. Askari, A. Adibi, P. J. Hotchkiss, S. C. Jones, S. R. Marder, R. A. Norwood and N. Peyghambarian, *Appl. Phys. Lett.*, 2007, **91**, 221109.

73 R. van der Heijden, C. F. Carlstrom, J. A. P. Snijders, R. W. van der Heijden, F. Karouta, R. Notzel, H. W. M. Salemink, B. K. C. Kjellander, C. W. M. Bastiaansen, D. J. Broer and E. van der Drift, *Appl. Phys. Lett.*, 2006, **88**, 161112.

74 K. Yoshino, Y. Shimoda, Y. Kawagishi, K. Nakayama and M. Ozaki, *Appl. Phys. Lett.*, 1999, **75**, 932.

75 B. Esembeson, M. L. Scimeca, T. Michinobu, F. Diederich and I. Biaggio, *Adv. Mater.*, 2008, **20**, 4584.

76 F. Qin, Z. M. Meng, X. L. Zhong, Y. Liu and Z. Y. Li, *Opt. Express*, 2012, **20**, 13091.

77 S. Y. Chou, P. R. Krauss and P. J. Renstrom, *Appl. Phys. Lett.*, 1995, **67**, 3114.

78 S. Y. Chou, P. R. Krauss and P. J. Renstrom, *J. Vac. Sci. Technol., B*, 1996, **14**, 4129.

79 E. M. Arakcheeva, E. M. Tanklevskaya, S. I. Nesterov, M. V. Maksimov, S. A. Gurevich, J. Seekamp and C. M. S. Torres, *Curr. Appl. Phys*, 2005, **50**, 1043.

80 C. G. Choi, C. S. Kee and H. Schift, *Curr. Appl. Phys.*, 2006, **6**, e8.

81 F. Qin, Y. Liu, Z. M. Meng and Z. Y. Li, *J. Appl. Phys.*, 2010, **108**, 053108.

82 L. Gan, Y. Z. Liu, J. Y. Li, Z. B. Zhang, D. Z. Zhang and Z. Y. Li, *Opt. Express*, 2009, **17**, 9962.

83 L. Gan, C. Z. Zhou, C. Wang, R. J. Liu, D. Z. Zhang and Z. Y. Li, *Phys. Status Solidi A*, 2010, **207**, 2715.

84 Y. Z. Liu, R. J. Liu, C. Z. Zhou, D. Z. Zhang and Z. Y. Li, *Opt. Express*, 2008, **16**, 21483.

85 Z. Y. Li, *Front. Phys.*, 2012, **7**, 601.

86 Y. Liu, F. Qin, F. Zhou, Q. B. Meng, D. Z. Zhang and Z. Y. Li, *Front. Phys. China*, 2010, **5**, 220.

87 M. R. Singh and R. H. Lipson, *J. Phys. B: At., Mol. Opt. Phys.*, 2008, **41**, 015401.

88 H. Dong, J. Gao, X. Kong, M. Cai and L. Shi, *Chin. Opt. Lett.*, 2007, **5**, 580.

89 R. R. Panepucci, B. H. Kim, V. R. Almeida and M. D. Jones, *J. Vac. Sci. Technol., B*, 2004, **22**, 3348.

90 J. Wülbern, M. Schmidt, U. Hübner, R. Boucher, W. Volksen, Y. Lu, R. Zentel and M. Eich, *Phys. Status Solidi A*, 2007, **204**, 3739.

This journal is © The Royal Society of Chemistry 2014

J. Mater. Chem. C, 2014, **2**, 783–800 | **799**

91 C. G. Choi, Y. T. Han, J. T. Kim and H. Schift, *Appl. Phys. Lett.*, 2007, **90**, 221109.

92 E. Pialat, T. Trigaud, J. P. Mouton and M. Thevenot, *J. Polym. Sci., Part B: Polym. Phys.*, 2007, **45**, 2993.

93 Z. M. Meng, X. L. Zhong, C. Wang and Z. Y. Li, *Chin. Opt. Lett.*, 2012, **10**, 112202.

94 Z. H. Li and G. F. Li, *IEEE Photonics Technol. Lett.*, 2006, **18**, 1341.

95 Y. A. Zaghloul and A. R. M. Zaghloul, *Opt. Express*, 2006, **14**, 9879.

96 J. I. Cirac and P. Zoller, *Nature*, 2000, **404**, 579.

97 Z. Zhao, A. N. Zhang, Y. A. Chen, H. Zhang, J. F. Du, T. Yang and J. W. Pan, *Phys. Rev. Lett.*, 2005, **94**, 030501.

98 J. Y. Kim, J. M. Kang, T. Y. Kim and S. K. Han, *Electron. Lett.*, 2006, **42**, 303.

99 Z. J. Li, Z. W. Chen and B. J. Li, *Opt. Express*, 2005, **13**, 1033.

100 L. A. Wang, S. H. Chang and Y. F. Lin, *Opt. Eng.*, 1998, **37**, 1011.

101 T. Fujisawa and M. Koshiba, *J. Opt. Soc. Am. B*, 2006, **23**, 684.

102 T. K. Liang, L. R. Nunes, M. Tsuchiya, K. S. Abedin, T. Miyazaki, D. Van Thourhout, W. Bogaerts, P. Dumon, R. Baets and H. K. Tsang, *Opt. Commun.*, 2006, **265**, 171.

103 V. M. Passaro and F. de Passaro, *Opt. Quantum Electron.*, 2006, **38**, 877.

104 Y. Liu, F. Qin, Z. M. Meng, F. Zhou, Q. H. Mao and Z. Y. Li, *Opt. Express*, 2011, **19**, 1945.

105 Y. Liu, F. Qin, F. Zhou and Z. Y. Li, *J. Appl. Phys.*, 2009, **106**, 083102.

106 Z. M. Meng, F. Qin, Y. Liu and Z. Y. Li, *J. Appl. Phys.*, 2011, **109**, 043107.

107 F. Qin, Y. Liu, Z. M. Meng and Z. Y. Li, *J. Appl. Phys.*, 2010, **108**, 053108.

108 Z. M. Meng, X. L. Zhong, C. Wang and Z. Y. Li, *Europhys. Lett.*, 2012, **98**, 54002.

109 Z. M. Meng, F. Qin and Z. Y. Li, *J. Opt.*, 2012, **14**, 065003.

110 F. Qin, Z. M. Meng and Z. Y. Li, *J. Opt. Soc. Am. B*, 2012, **29**, 2314.

111 F. Zhou, Y. Liu, Z. Y. Li and Y. N. Xia, *Opt. Express*, 2010, **18**, 13337.

112 Y. K. Gong, Z. Y. Li, J. X. Fu, Y. H. Chen, G. X. Wang, H. Lu, L. R. Wang and X. M. Liu, *Opt. Express*, 2011, **19**, 10193.